

# Structural and Computational Characterization of the SHV-1 $\beta$ -Lactamase- $\beta$ -Lactamase Inhibitor Protein Interface<sup>\*S</sup>

Received for publication, April 24, 2006, and in revised form, June 21, 2006. Published, JBC Papers in Press, June 29, 2006, DOI 10.1074/jbc.M603878200

Kimberly A. Reynolds<sup>†S1</sup>, Jodi M. Thomson<sup>¶2</sup>, Kevin D. Corbett<sup>||</sup>, Christopher R. Bethel<sup>\*\*</sup>, James M. Berger<sup>||</sup>, Jack F. Kirsch<sup>||3</sup>, Robert A. Bonomo<sup>†\*\*4</sup>, and Tracy M. Handel<sup>†5</sup>

From the <sup>†</sup>Skaggs School of Pharmacy and Pharmaceutical Sciences, University of California San Diego, La Jolla, California 92093-0684, the <sup>¶</sup>Department of Pharmacology, Case Western Reserve University, Cleveland, Ohio 44106, the <sup>§</sup>Biophysics Group and <sup>||</sup>Department of Molecular and Cell Biology, University of California, Berkeley, California 94720, and <sup>\*\*</sup>Research Service, Louis Stokes Veterans Affairs Medical Center, Cleveland, Ohio 44106

$\beta$ -Lactamase inhibitor protein (BLIP) binds a variety of class A  $\beta$ -lactamases with affinities ranging from micromolar to picomolar. Whereas the TEM-1 and SHV-1  $\beta$ -lactamases are almost structurally identical, BLIP binds TEM-1 ~1000-fold tighter than SHV-1. Determining the underlying source of this affinity difference is important for understanding the molecular basis of  $\beta$ -lactamase inhibition and mechanisms of protein-protein interface specificity and affinity. Here we present the 1.6 Å resolution crystal structure of SHV-1·BLIP. In addition, a point mutation was identified, SHV D104E, that increases SHV·BLIP binding affinity from micromolar to nanomolar. Comparison of the SHV-1·BLIP structure with the published TEM-1·BLIP structure suggests that the increased volume of Glu-104 stabilizes a key binding loop in the interface. Solution of the 1.8 Å SHV D104K·BLIP crystal structure identifies a novel conformation in which this binding loop is removed from the interface. Using these structural data, we evaluated the ability of EGAD, a program developed for computational protein design, to calculate changes in the stability of mutant  $\beta$ -lactamase·BLIP complexes. Changes in binding affinity were calculated within an error of 1.6 kcal/mol of the experimental values for 112 mutations at the TEM-1·BLIP interface and within an error of 2.2 kcal/mol for 24 mutations at the SHV-1·BLIP interface. The reasonable success of EGAD in predicting changes in interface stability is a promising step toward understanding the stability of the  $\beta$ -lactamase·BLIP complexes and computationally assisted design of tight binding BLIP variants.

Class A  $\beta$ -lactamases are a major cause of  $\beta$ -lactam resistance in Gram-negative bacteria. These enzymes catalyze the hydrolysis of  $\beta$ -lactam antibiotics, such as penicillins and cephalosporins, rendering them inactive.  $\beta$ -Lactamase inhibitor protein (BLIP),<sup>6</sup> which is secreted by the Gram-positive soil bacterium *Streptomyces clavuligeris*, inhibits a variety of class A  $\beta$ -lactamase enzymes with a wide spectrum of affinities. Its binding partners include *Escherichia coli* TEM-1, *Klebsiella pneumoniae* SHV-1, *Serratia marcescens* SME-1, *Bacillus anthracis* BlaI, and *Proteus vulgaris* K1, among others. BLIP is able to inhibit K1 with picomolar affinity and TEM-1, SME-1, and BlaI with nanomolar affinity. However, it inhibits SHV-1 with only micromolar affinity (1, 2). Whereas SHV-1 shares 67% sequence identity with TEM-1 (Fig. 1), and the crystal structures of the unbound  $\beta$ -lactamases overlay with an  $\alpha$ -carbon r.m.s. deviation of 1.4 Å, BLIP exhibits a 1000-fold difference in affinity for the two (3). This poses an interesting question of binding specificity and affinity. How does BLIP bind multiple targets, and what is the source of variation in binding affinity? Recent alanine scanning mutagenesis has provided insight into the origins of BLIP affinity and specificity for an array of  $\beta$ -lactamases, including TEM-1 and SHV-1 (2, 4). However, interpretation of these data has been limited, because only the structure of the TEM-1·BLIP complex has been solved by x-ray crystallography (5).

Alanine-scanning mutagenesis and comparison of unbound crystal structures suggested that class A  $\beta$ -lactamase residue 104 (Ambler numbering system) (6), which is a glutamate in TEM-1 and an aspartate in SHV-1, plays a key role in mediating BLIP affinity. It has been hypothesized that the reduced volume of aspartate disrupts the interfacial salt bridge seen between Glu-104<sub>TEM-1</sub> and Lys-74<sub>BLIP</sub> and moves the carboxylate group of Asp-104<sub>SHV-1</sub> closer to Glu-73<sub>BLIP</sub>, introducing an electrostatic clash (2, 3). Interestingly, the TEM E104K mutation decreases affinity for BLIP from 0.11 to 140 nM (7). By contrast, we found that the analogous D104K mutation in SHV has little effect on binding affinity (582 nM for SHV D104K·BLIP *versus*

\* The costs of publication of this article were defrayed in part by the payment of page charges. This article must therefore be hereby marked "advertisement" in accordance with 18 U.S.C. Section 1734 solely to indicate this fact. The atomic coordinates and structure factors (code 2G2U and 2G2W) have been deposited in the Protein Data Bank, Research Collaboratory for Structural Bioinformatics, Rutgers University, New Brunswick, NJ (<http://www.rcsb.org/>).

<sup>S</sup> The on-line version of this article (available at <http://www.jbc.org>) contains supplemental Tables 1 and 2.

<sup>1</sup> Supported by a National Science Foundation (NSF) graduate research fellowship.

<sup>2</sup> Supported in part by National Institutes of Health (NIH) Grant T32 GM07250 and by the Case Medical Scientist Training Program.

<sup>3</sup> Supported by NIH Grant GM35393.

<sup>4</sup> Supported by NIH Grant 5R01AI635172 and the Veterans Affairs Medical Center Merit Review Program.

<sup>5</sup> Supported by NSF Grant 0344749. To whom correspondence should be addressed: CMM East Rm. 2057, 9500 Gilman Dr. Mail Code 0684, La Jolla, CA 92093-0684. Tel.: 858-822-6656; Fax: 858-822-6655; E-mail: [thandel@ucsd.edu](mailto:thandel@ucsd.edu).

<sup>6</sup> The abbreviations used are: BLIP,  $\beta$ -lactamase inhibitor protein; vdW, van der Waals; r.m.s., root mean square; BisTris, 2-[bis(2-hydroxyethyl)amino]-2-(hydroxymethyl)propane-1,3-diol.

## Characterization of the SHV-1·BLIP Interface

**A.**

TEM-1	HPETLVKVKDAEDQLGARVGYIELDLNSGKILESFRPEERFPMSTFKVLLCGAVLSRID	85
SHV-1	SPQPLEQIKLSQESQLSGRVGMIEMDLASEGRITLAWRADERFPMSTFKVLLCGAVLARVD	85
TEM-1	AGQEQLGRRIHYSQNDLVEYSPVTEKHLTDGMTVRELCSAAITMSDNTAANLLLTITGGP	145
SHV-1	AGDEQLERKIHYSROODLVEYSPVSEKHLADGMTVRELCSAAITMSDNTAANLLLATVGGP	145
TEM-1	KELTAFLHNMGDHVTSLDRWPELNEATPNDERDTMPVAMATTLRKLTLGELLTLASRQ	205
SHV-1	AGLTAFLRQIGDNVTSLDRWPELNEALPGDARDTTPASMAATTLRKLTLTSQLRSARSQR	205
TEM-1	QLIDWMEADKLVAGPLLRSAIPAGWFIADKSGAGERGSRGIIAALGPDGKPSRIVVIYTTG	267
SHV-1	QLLQWVMDRIRVAGPLLRVLPAGWFIADKSGAGERGARGIVALLGPNNKAERIVVIYLRD	267
TEM-1	SQATMDERNRQIAETGASLIKHW--	292
SHV-1	TPASMAERNQQIAGIGAAALIEHWQR	292

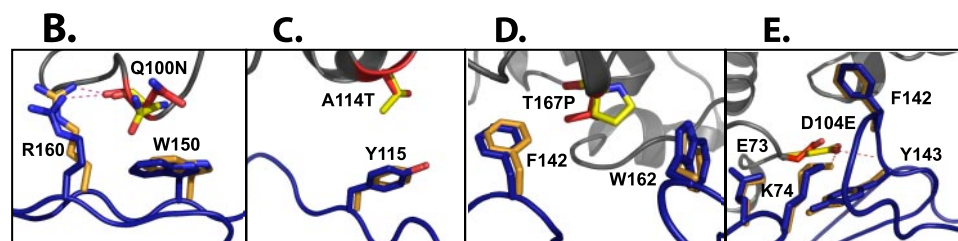


**FIGURE 1. Comparison of amino acid differences at the SHV-1·BLIP and TEM-1·BLIP interfaces.** *A*, sequence alignment of TEM-1 and SHV-1 (Ambler numbering system). Conserved residues are highlighted in light gray, conserved interface residues in dark gray, and nonconserved interface residues in orange. Interface residues were defined as  $\beta$ -lactamase residues within 6 Å of BLIP. SHV-1 and TEM-1 share 67% sequence identity overall and 81% at interface residues. *B–E*, structural alignment of interface amino acid positions differing between SHV-1 and TEM-1. For clarity, only the backbone coordinates of SHV-1 and BLIP bound to SHV-1 are shown. The SHV-1 side chain is shown in red, the TEM-1 side chain in yellow, BLIP bound to SHV-1 in dark blue, and BLIP bound to TEM-1 in orange. *B*, structural overlay of SHV-1 Gln-100 and TEM-1 Asn-100. *C*, structural overlay of SHV-1 Ala-114 and TEM-1 Thr-114. *D*, structural overlay of SHV-1 Thr-167 and TEM-1 Pro-167. *E*, structural overlay of SHV-1 Asp-104 and TEM-1 Glu-104.

**TABLE 1**

Summary of  $\beta$ -lactamase·BLIP  $K_d$  determinations for  $\beta$ -lactamase position 104 mutants

The wild type identity of position 104 is glutamate in TEM-1, aspartate in SHV-1, and lysine in an extended spectrum TEM variant. ND, not determined.

Mutation	TEM-1·BLIP $K_d$	SHV-1·BLIP $K_d$
HM	HM	HM
Glu-104	$0.32 \pm 0.03$	$1.1 \pm 0.1$
Asp-104	ND	$1252 \pm 52$
Lys-104	$140 \pm 5^a$	$582 \pm 42$

<sup>a</sup> Value from Ref. 7.

1252 nM for SHV-1·BLIP), and the D104E mutation increases affinity to 1.1 nM (Table 1). To understand the basis of these affinity differences, we solved the structures of the SHV-1·BLIP and SHV D104K·BLIP complexes to 1.6 and 1.8 Å, respectively (Table 2).

Although crystal structures provide a physical model that can be visualized, a thorough understanding of binding specificity and affinity also requires analysis of the energetics underlying interface stabilization. In turn, by understanding the physical forces involved in protein complex formation, the design of tight binding protein partners with desired specificities should become feasible. The TEM-1·BLIP interface has already been demonstrated to be an excellent system for dissecting and re-engineering protein-protein interactions; both the Schreiber and Tidor groups (8–10) have examined the effects of electrostatic interactions on the stability of this complex. To further

interpret the mutational data in the context of structure, we used EGAD, our protein design algorithm, to calculate changes in binding affinity for an extensive set of experimentally characterized TEM-1·BLIP and SHV-1·BLIP mutants (2, 7, 9, 11–14). This energy function was previously shown to predict relative affinities for a large set of protein interface mutational data, including a reduced set of TEM-1 mutants, correctly (15). The present calculations extend this work to a larger set of TEM-1·BLIP mutations as well as to the SHV-1·BLIP interface. The reasonable success of these predictions indicates that EGAD can be used to guide further mutational analysis of the  $\beta$ -lactamase·BLIP complexes, including creation of tighter binding variants. Whereas the  $\beta$ -lactamase·BLIP complexes were chosen as model systems, a combined approach of structural, computational, and mutagenic techniques is emerging as a powerful method for engineering protein variants with potential for medical and other scientific applications.

## EXPERIMENTAL PROCEDURES

**Cloning and Protein Purification**—The *bla*<sub>SHV</sub> gene cloned into pBC SK(–) phagemid (Stratagene, La Jolla, CA) was used to construct the *bla*<sub>D104K</sub> and *bla*<sub>D104E</sub> variants of SHV-1  $\beta$ -lactamase (16, 17). The *bla*<sub>D104E</sub> mutation was created in pBC SK(–), whereas the *bla*<sub>D104K</sub> variant was subcloned into pET-24a(+) (Novagen, Madison, WI). Mutagenesis was then performed at position 104 using the QuikChange® site-directed mutagenesis kit (Stratagene).

SHV-1 and SHV D104E were expressed in pBC SK(–) in *E. coli* DH10B cells grown overnight, without induction. SHV D104K was expressed in *E. coli* BL21(DE3) cells by induction with 0.2 mM isopropyl- $\beta$ -D-thiogalactopyranoside at  $A_{600} = 0.8$  for 3 h at 37 °C. For all enzymes, cells were harvested by centrifugation at 4 °C and frozen overnight.  $\beta$ -Lactamase was liberated using stringent periplasmic fractionation with lysozyme and EDTA as previously described (18). Preparative isoelectric focusing was performed with a Sephadex granulated gel and ampholines in the pH range of 3.5–10 (Amersham Biosciences). The protein was eluted with 20 mM diethanolamine buffer, pH 8.3. An additional HPLC purification step was performed on a Waters high pressure liquid chromatograph using a Sephadex Hi Load 26/60 column (Amersham Biosciences) and eluted with phosphate-buffered saline (pH 7.4). This expression and purification scheme yielded ~10 mg of pure protein/liter of culture for SHV-1 and SHV D104E and 1 mg for SHV D104K.

**TABLE 2**
**Data collection, refinement, and stereochemistry for the SHV-1:BLIP and SHV D104K:BLIP structures**
 $R_{\text{sym}} = \frac{\sum \sum |I_j - \langle I \rangle|}{\sum I_j}$ , where  $I_j$  is the intensity measurement for reflection  $j$ , and  $\langle I \rangle$  is the mean intensity for multiple recorded reflections.  $R_{\text{work, free}} = \frac{\sum ||F_o| - |F_c||}{\sum |F_o|}$ , where the working and free  $R$ -factors are calculated using the working and free reflection sets, respectively. The free reflections were held aside throughout refinement.

Parameters	Values	
	SHV-1·BLIP	SHV D104K·BLIP
<b>Data collection</b>		
Resolution (Å)	30.0-1.6	30.0-1.8
Wavelength (Å)	1.1159	1.1159
Space group	P63	P1
Unit cell dimensions ( <i>a</i> , <i>b</i> , <i>c</i> ) (Å)	127.87, 127.87, 73.40	42.56, 44.83, 62.90
Unit cell angles ( $\alpha$ , $\beta$ , $\gamma$ ) (degrees)	90.0, 90.0, 120.0	78.88, 88.95, 62.42
<i>I</i> / $\sigma$ (last shell)	34.9 (5.28)	25.4 (6.07)
$R_{\text{sym}}$ (last shell) (%)	0.055 (0.305)	0.030 (0.096)
Completeness (last shell) %	98.7 (97.2)	95.9 (89.7)
No. of reflections	1,227,626	179,431
No. of unique reflections	88,872	35,776
<b>Refinement</b>		
Resolution (Å)	30.0-1.6	30.0-1.8
No. of reflections	88,841	35,772
No. of working reflections	84,358	33,986
No. of free reflections (% of total)	4483 (5%)	1786 (5%)
$R_{\text{work}}$ (last shell) (%)	17.29 (15.9)	18.0 (22.2)
$R_{\text{free}}$ (last shell) (%)	18.61 (19.8)	21.4 (25.7)
<b>Structure and stereochemistry</b>		
No. of atoms	3590	3447
No. of protein atoms	3259	3254
No. of waters	331	193
r.m.s. deviation bond lengths (Å)	0.012	0.010
r.m.s. deviation bond angles (degrees)	1.37	1.21

TEM-1 cloned into pET24a(+) with a N-terminal OmpA secretion signal was provided by Stéphane Gagné (Université Laval). TEM-1 was expressed and purified as in Ref. 19. The BLIP construct was a generous gift from Susan Jensen (University of Alberta). The BLIP *bli* gene was cloned into pET26b (Novagen, Madison, WI), with the native *S. clavuligeris* signal sequence at the N terminus. BLIP was expressed in *E. coli* BL21(DE3) cells by inducing with 1 mM isopropyl- $\beta$ -D-thiogalactopyranoside at  $A_{600} = 0.5$  for 3 h at 30 °C. Cells were harvested by centrifugation, resuspended in 20 g/100 ml sucrose, 1 mM EDTA, 30 mM Tris, pH 8.0, and incubated for 15 min. The cells were pelleted and resuspended in 5 mM MgCl<sub>2</sub>. After centrifugation at 7,000 rpm for 10 min, the periplasmic fraction was retained, and a Complete protease inhibitor mixture tablet (Roche Applied Science) was added. That fraction was subsequently clarified by additional centrifugation and loaded onto a HiPrep 16/10 Q-XL anion exchange column (Amersham Biosciences) equilibrated in 25 mM Tris, pH 8.4, 1 mM EDTA. A 250-ml gradient from 0 to 500 mM NaCl was used to isolate BLIP, which elutes at ~150 mM NaCl. Fractions were pooled and concentrated to a final volume of ~2 ml and subsequently passed through a HiLoad 26/60 Superdex 75 preparation grade gel filtration column (Amersham Biosciences) equilibrated in 50 mM Tris, pH 8.4, 100 mM NaCl. After purification, BLIP was concentrated to 1 mg/ml and stored at -80 °C. This expression and purification scheme yielded roughly 0.5 mg of pure protein/liter of culture.

**Crystallization, Data Collection, and Structure Solution**—SHV-1 or SHV D104K was mixed 1:1 with BLIP in 20 mM BisTris, pH 7.25, 50 mM NaCl, concentrated to 8.7 mg/ml, and dialyzed overnight against 20 mM BisTris, pH 7.25, 50 mM NaCl. Crystals were grown at 19 °C in microbatch format under Al's oil (Hamp-ton Research, Aliso Viejo, CA) by mixing 1  $\mu$ l of protein with 1  $\mu$ l of well solution. The SHV-1·BLIP crystals were grown in a well solution of 60% ammonium sulfate, 50 mM cacodylate, pH 6.5; SHV D104K·BLIP crystals were grown in a well solution of 8% polyethylene glycol 8000, 50 mM cacodylate, pH 6.5. For harvesting, a cryoprotectant solution containing well solution plus 25% glycerol for SHV-1·BLIP or well solution plus 30% xylitol for SHV D104K·BLIP was added directly to the drop, and the crystals were immediately looped and flash-frozen in liquid nitrogen.

Data sets were collected on Beamline 8.3.1 at the Advanced Light Source at Lawrence Berkeley National Laboratory (20). A preliminary 2.1 Å data set for SHV-1·BLIP was collected on an R-Axis IV++ at the University of California Berkeley (Rigaku/ MSC, The Woodlands, TX). Data were indexed and reduced with HKL2000 (21) or ELVES (22) using MOSFLM (23). For the 1.8 Å high resolution SHV-1·BLIP structure, molecular replacement was performed using a partially refined structure from the 2.1 Å data set. Initial maps for the SHV D104K·BLIP structure were generated by molecular replacement with PHASER (24) using polyalanine models of SHV-1 (coordinates taken from Protein Data Bank entry 1SHV) and BLIP (coordinates taken from Protein Data Bank entry 1JTG) (3, 5). Manual rebuilding was carried out with O (25). Refinement was carried out with Refmac (26) using ARP to automatically place ordered waters, followed by TLS refinement (27). Additional details of the data collection and refinement are provided in Table 2. Structural alignments and r.m.s. deviations were calculated with LSQMAN (28). All molecular figures were created with PyMOL (29).

**Inhibition Assays**—All kinetic determinations were performed using nitrocefin (BD Biosciences) as the indicator substrate to measure hydrolysis rates of SHV-1, SHV D104K, SHV D104E, and TEM-1  $\beta$ -lactamases with and without inhibitor. BLIP and lactamase were incubated for 2 h at room temperature in 10 mM sodium phosphate-buffered saline containing 1 mg/ml bovine serum albumin. Initially, 7 nM enzyme was used for all assays, but this was reduced to 4 nM for SHV D104E and 2 nM for TEM-1 to obtain an accurate measurement of the low  $K_d$  values. Reactions were initiated with nitrocefin at the  $K_m$  for the enzyme (25  $\mu$ M for SHV-1, 15  $\mu$ M for SHV D104K, 25  $\mu$ M for SHV D104E, and 150  $\mu$ M for TEM-1). Final reaction volumes were 1 ml. All measurements were performed in triplicate. Hydrolysis rates were determined at  $\lambda = 482$  nm using the extinction coefficient,  $\epsilon = 17,400 \text{ M}^{-1} \text{ cm}^{-1}$  for the hydrolyzed form of nitrocefin (30).

BLIP inhibition curves were graphed using Origin® 7.5 SR software and fit to the following equation,

$$E_{\text{free}} = [E_0] - \frac{[E_0] + [I_0] + K_d^* - \sqrt{([E_0] + [I_0] + K_d^*)^2 - (4[E_0][I_0])}}{2} \quad (\text{Eq. 1})$$

where  $E_{\text{free}}$  represents the remaining free enzyme concentration calculated based on activity,  $[E_0]$  is initial enzyme concen-

## Characterization of the SHV-1·BLIP Interface

tration,  $[I_0]$  is the concentration of BLIP, and  $K_d^*$  is the apparent equilibrium constant (7).  $K_d^*$  was corrected for the presence of substrate using the following equation.

$$K_d = \frac{K_d^*}{(1 + [S]/K_m)} \quad (\text{Eq. 2})$$

**Computational Calculation of Free Energies of Dissociation—**EGAD\_lib,<sup>7</sup> a C++ implementation of the EGAD protein design energy function, was employed to calculate dissociation free energies of the complexes (15, 31). The function consists of an OPLS-AA derived force field (32) alongside a solvent-accessible surface area term and the generalized Born model to describe solvation. The force field terms include a linearized van der Waals (vdW) potential, a coulombic electrostatics term, and a torsional potential. Minimization was conducted using Monte Carlo simulated annealing followed by a heuristic quench step (15).

An initial model for the bound state of the complex was created by rotamer optimization of the corresponding crystal structure (Protein Data Bank code 1JTG for TEM-1·BLIP, Protein Data Bank code 2G2U for SHV-1·BLIP, or Protein Data Bank code 2G2W for SHV D104K·BLIP) (45). The unbound state model was generated by separating the two chains in the complex by 25 Å, followed by rotamer optimization of each. For these complexes, calculations performed with the rotamer-optimized initial model were not significantly different from those using the Protein Data Bank structure directly. Typically, we use initial rotamer optimization in interface calculations as a precaution against improperly refined rotamers, although the high resolution of the  $\beta$ -lactamase·BLIP structures makes this step less important.

The free energy of dissociation is defined as the energy difference between the complex and free states.

$$\Delta G_d = \Delta G_{\text{bound}} - \Delta G_{\text{free}} \quad (\text{Eq. 3})$$

The free energy used for comparison with experimental values is as follows.

$$\Delta\Delta G_{d, \text{mut}} = \eta(\Delta G_{d, \text{mut}} - \Delta G_{d, \text{WT}}) \quad (\text{Eq. 4})$$

Here  $\eta$  is a scaling factor used to normalize the predicted changes in binding affinity to have a slope of 1 when compared with the experimental energy changes (15). For  $\Delta\Delta G_{d, \text{mut}}$  calculated with the TEM-1·BLIP backbone coordinates,  $\eta = 0.18$ ; for both SHV-1·BLIP and SHV D104K·BLIP,  $\eta = 0.30$ . The mutant free energies were calculated by rotamer optimization of the mutant structures, allowing only a reduced set of positions to move during optimization. This set was restricted to residues at the interface (residues that undergo a change in solvent-accessible surface area upon binding) and their neighbors.

## RESULTS

**Structure of the SHV-1·BLIP Complex—**The structure of the SHV-1·BLIP complex is globally similar to that of TEM-1·BLIP; alignment of the  $\alpha$ -carbon atoms of TEM-1 and SHV-1 yields

an r.m.s. deviation of 0.44 Å between the two  $\beta$ -lactamases and an r.m.s. deviation of 1.04 Å between the associated BLIPs (Fig. 2). Alignment of all  $\alpha$ -carbon atoms yields an overall r.m.s. deviation of 0.61 Å for the two complexes. As in the TEM-1 complex, the concave  $\beta$ -sheet region of BLIP latches onto a protruding loop-helix region of SHV-1 (residues 99–112), and two loops of BLIP insert into the  $\beta$ -lactamase active site. Residues Asp-49 (at the end of the first loop) and Phe-142 (at the end of the second loop) form an approximate mimic of the  $\beta$ -lactamase substrate, penicillin G (5). Comparison of the bound and unbound forms of SHV-1 reveals only minimal global changes in conformation upon binding, with the exception of the H10 helix (residues 218–230) (Fig. 3). In the SHV-1·BLIP structure, the H10 helix partially unravels at the N terminus, assuming a structure similar to the H10 helix as observed in both the bound and unbound forms of TEM-1. The H10 helix conformation in the crystal of unbound SHV-1 is possibly affected by proximal binding of a detergent molecule, Cymal-6 (3). Previously, it was observed that the conformation of the H10 helix interacting with detergent in the SHV-1 unbound structure was similar to the conformational change seen when TEM-1 interacts with an allosteric cryptic site inhibitor (33).

The question then remains, what features are responsible for the differential affinity of BLIP for TEM-1 *versus* SHV-1? There are eight SHV-1 residues within 6 Å of BLIP that differ in identity from TEM-1 (Fig. 1A). These include R98S, Q100N, D104E, A114T, S133T, T167P, R215K, and T235S (here the residue identity in SHV-1 is listed first). Comparison of the hydrogen bond, salt bridge, and vdW interactions of these residues in the TEM-1·BLIP and SHV-1·BLIP complexes provides some structural insight. EGAD was used to quantify the extent of vdW contact. Pairwise vdW energies were calculated between all interface residues, and those providing stabilizing interactions in excess of  $-1.0$  kcal/mol are tabulated in supplemental Table 2. A combination of the REDUCE and BndList programs was used to detect hydrogen bonds and salt bridges (34) (supplemental Table 1). In a few cases, the SHV-1 residue type contributes new interactions: Arg-98<sub>SHV</sub> has improved vdW packing with Trp-150<sub>BLIP</sub> relative to Ser-98<sub>TEM</sub>, and Arg-215<sub>SHV</sub> forms two hydrogen bonds with Glu-31<sub>BLIP</sub>, whereas Lys-215<sub>TEM</sub> forms only one. For positions 133 and 235, there is little difference between the TEM-1 and SHV-1 residues; S133T makes few interfacial contacts in SHV-1 or TEM-1, and Thr-235<sub>SHV</sub> forms a hydrogen bond with Asp-49<sub>BLIP</sub> analogous to that formed by Ser-235<sub>TEM</sub>. However, for the remaining four residue differences, TEM-1 forms more extensive interactions across the interface. The backbone carbonyls of Gln-100<sub>SHV</sub> and Asn-100<sub>TEM</sub> both form a hydrogen bond with Arg-160<sub>BLIP</sub>, although Asn-100<sub>TEM</sub> is able to form more extensive vdW contacts with Trp-150<sub>BLIP</sub> and Arg-160<sub>BLIP</sub> (Fig. 1B). Thr-114<sub>TEM</sub> exhibits improved vdW interactions with Tyr-115<sub>BLIP</sub> in comparison with Ala-114<sub>SHV</sub> (Fig. 1C), and Pro-167<sub>TEM</sub> forms more extensive contacts with Trp-162<sub>BLIP</sub>; however, Thr-167<sub>SHV</sub> does provide increased vdW interactions with Phe-142<sub>BLIP</sub> (Fig. 1D). The reduced volume of Asp-104<sub>SHV</sub> eliminates the interfacial salt bridge between Glu-104<sub>TEM</sub> and Lys-74<sub>BLIP</sub>. A hydrogen bonding interaction between Glu-104<sub>TEM</sub> and the Tyr-143<sub>BLIP</sub> backbone is not formed with Asp-104<sub>SHV</sub>, favorable vdW packing interactions between Glu-104<sub>TEM</sub> and Phe-

<sup>7</sup> A. Chowdry, K. A. Reynolds, M. S. Voorhies, M. S. Hanes, N. Pokala, and T. M. Handel, manuscript in preparation.

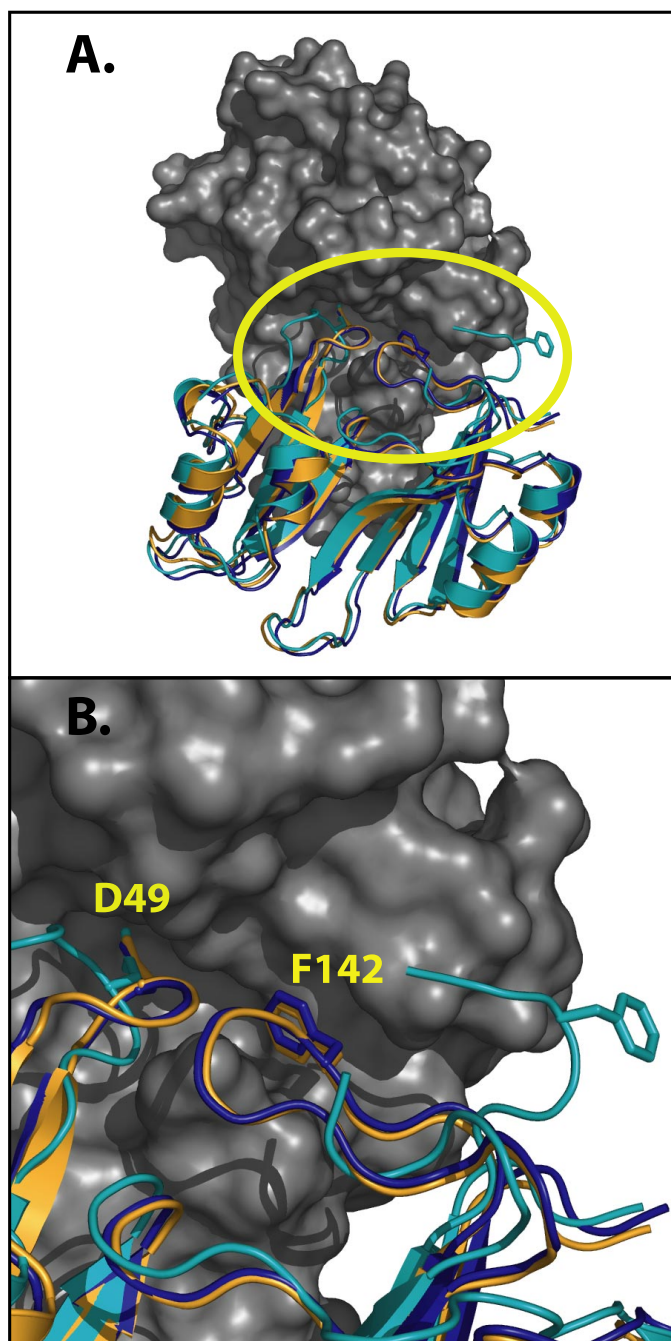


**FIGURE 2. Comparison of the BLIP complexes with TEM-1, SHV-1, and SHV D104K.** All structures were constructed by  $\alpha$ -carbon alignment of the two  $\beta$ -lactamases. For clarity, the bound BLIPs are shown in reference to the SHV-1 structure only, since all three  $\beta$ -lactamases align within an average  $\alpha$ -carbon r.m.s. deviation of 0.41 Å. The  $\beta$ -lactamase is shown in gray, BLIP bound to TEM-1 in orange, BLIP bound to SHV-1 in dark blue, and BLIP bound to SHV D104K in cyan. The TEM-1- and SHV-1-bound BLIP structures align with an  $\alpha$ -carbon r.m.s. deviation of 1.04 Å (A) with very little difference in the Asp-49 and Phe-142 binding loops (B). The SHV-1- and SHV D104K-bound BLIP structures align with an  $\alpha$ -carbon r.m.s. deviation of 2.24 Å (A) with large rearrangements in the Asp-49 and Phe-142 binding loops (B).

$142_{\text{BLIP}}$  are entirely eliminated in the SHV-1·BLIP interface, and the packing between Asp-104<sub>SHV</sub> and Tyr-143<sub>BLIP</sub> is significantly reduced relative to Glu-104<sub>TEM</sub> (Fig. 1E). These dramatic changes between position 104 in SHV-1 compared with TEM-1 suggest that it might be a particularly important hot spot in the interface.

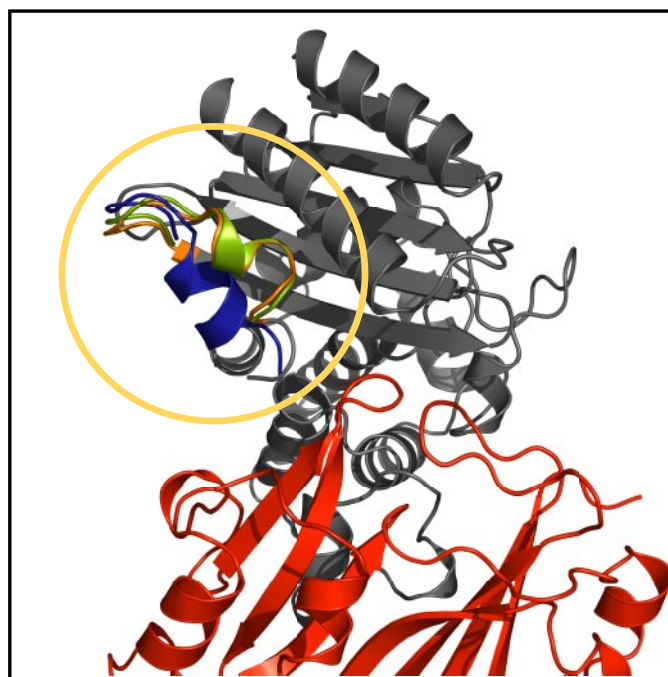


**FIGURE 3. Conformational change of the H10 helix.** The H10 helix of SHV-1 assumes an alternate conformation in the BLIP bound structure (shown in bright green). Here it is compared with the H10 helix of unbound SHV-1 in dark blue and of TEM-1 in orange. The conformation of the H10 helix is identical in both TEM-1 bound and unbound. The backbone coordinates of TEM-1 (in gray) bound to BLIP (in red) are shown for reference.

*Mutagenesis of SHV Position 104*—The substitution of aspartate in SHV-1 for glutamate in TEM-1 at position 104 shortens the side chain by a single carbon, yet a number of interactions across the  $\beta$ -lactamase·BLIP interface are eliminated. The loss of the Glu-104<sub>TEM</sub> and Lys-74<sub>BLIP</sub> salt bridge results in the energetically unfavorable burial of unsatisfied charges at the interface. The extensive contacts removed between position 104 and the Phe-142 loop are consistent with previous mutational data indicating that Phe-142<sub>TEM</sub> is a hot spot at the TEM-1·BLIP interface, whereas Phe-142<sub>SHV</sub> appears to have a reduced role in the SHV-1·BLIP interface (2). For these reasons, we further explored the role of position 104 at the SHV-1·BLIP interface through mutagenesis.

Remarkably, we find that the point mutant SHV D104E results in a 1000-fold increase in the binding affinity of BLIP (Table 1). The D104E substitution in SHV-1 may function to restore the salt bridge with Lys-74<sub>BLIP</sub> and, perhaps more importantly, provide stabilizing interactions with the Phe-142 loop. We are currently conducting further characterization of the SHV D104E mutation through crystallography and a more extensive double mutant cycle analysis.

In addition to the SHV D104E mutation, the SHV D104K mutation was characterized. The analogous TEM E104K mutation leads to an extended spectrum resistance phenotype and was previously found to decrease TEM-1 affinity for BLIP from 0.11 to 140 nM (7). However, we find that the SHV D104K mutation leads to a moderate increase in affinity, from 1252 to 582 nM. Interestingly, crystallography of this complex identifies an alternate BLIP binding mode.

*Structure of the SHV D104K·BLIP Complex*—In the SHV-1·BLIP structure, the Asp-49 and Phe-142 loops occupy the active

## Characterization of the SHV-1·BLIP Interface

site as in TEM-1. However, in the SHV D104K mutant complex, the Phe-142 loop swings out of the active site cavity, and the Asp-49 loop is rotated to partially occupy the space vacated by the Phe-142 loop (Fig. 2). Whereas the wild type binding mode buries an extent of surface area comparable with the TEM-1 complex (2757 Å<sup>2</sup> in TEM-1 versus 2624 Å<sup>2</sup> in SHV-1), the mutant buries only 2450 Å<sup>2</sup>. Curiously, despite the loss of interactions with the Phe-142 loop and the decreased amount of interfacial buried surface area, we find the SHV D104K interface to be slightly stabilized relative to the native complex (Table 1).

The removal of the Phe-142 loop from the SHV active site is the most striking difference between the wild type and D104K complexes (Fig. 2). The loop is somewhat disordered, and the density for BLIP residue 139 is missing entirely in the mutant complex. The loop forms a small number of crystal contacts with a neighboring SHV D104K·BLIP complex, consisting of two potential hydrogen bonds between Tyr-143<sub>BLIP</sub> and the neighboring SHV Gln-206 and Trp-110. When Lys-104<sub>SHV</sub> is modeled into the wild type SHV-1·BLIP complex using EGAD, a clash is introduced with Tyr-143<sub>BLIP</sub>. By swinging out of the active site, the Phe-142 loop relieves this collision. The removal of the flexible Phe-142 loop from the interface may serve to increase the overall entropy of the complex. However, all vdW contacts between the BLIP Phe-142 loop and SHV are lost when the Phe-142 loop is not present (supplemental Table 2). Instead, these lost interactions appear to be compensated for by increased interactions with the Asp-49 loop.

The interface hot spot residue Asp-49<sub>BLIP</sub> appears in almost identical conformations in the TEM-1·BLIP, SHV-1·BLIP, and SHV D104K·BLIP structures (Fig. 2). The average r.m.s. deviation for all possible pairwise comparisons between Asp-49<sub>BLIP</sub> in the three structures is 0.98 Å. In each case, Asp-49<sub>BLIP</sub> forms two salt bridges with Arg-244<sub>SHV</sub> and Lys-234<sub>SHV</sub>, as well as making two hydrogen bonds with Ser-130<sub>SHV</sub> and Thr-235<sub>SHV</sub> (Ser-235<sub>TEM</sub>). This positioning is consistent with its shared role as a hot spot in both the TEM-1·BLIP and SHV-1·BLIP interfaces (2, 12). Despite the highly conserved structural role of Asp-49<sub>BLIP</sub> in SHV D104K, the remainder of this loop is able to pivot around this residue, rotating further into the  $\beta$ -lactamase active site (Fig. 4). This allows the Tyr-50<sub>BLIP</sub> side chain to swing into the space vacated by loop residue Phe-142<sub>BLIP</sub>, creating two new interactions: a hydrogen bond between Tyr-50<sub>BLIP</sub> and Asn-132<sub>SHV</sub> and a possible  $\pi$  interaction between Asn-132<sub>SHV</sub> and the aromatic face of Tyr-50<sub>BLIP</sub>. In concert with the Tyr-50<sub>BLIP</sub> movement, residue Tyr-105<sub>SHV</sub> must swivel to the other side of the loop to avoid clashing with Tyr-50<sub>BLIP</sub>. This rearrangement breaks a hydrogen bond between Tyr-105<sub>SHV</sub> and Gly-141<sub>BLIP</sub> (located in the Phe-142 loop) and creates a new hydrogen bond between Tyr-105<sub>SHV</sub> and Tyr-51<sub>BLIP</sub> (supplemental Table 1).

The concerted movement between Tyr-50<sub>BLIP</sub> and Tyr-105<sub>SHV</sub> also changes the vdW packing at the interface (supplemental Table 2). Tyr-105<sub>SHV</sub> no longer forms stabilizing vdW contacts with Phe-142<sub>BLIP</sub> but now interacts with Tyr-51<sub>BLIP</sub> and Tyr-53<sub>BLIP</sub> in the Asp-49 loop, as well as forming more extensive interactions with Tyr-50<sub>BLIP</sub>. The repositioning of Tyr-105<sub>SHV</sub> is similar to that observed in the TEM1

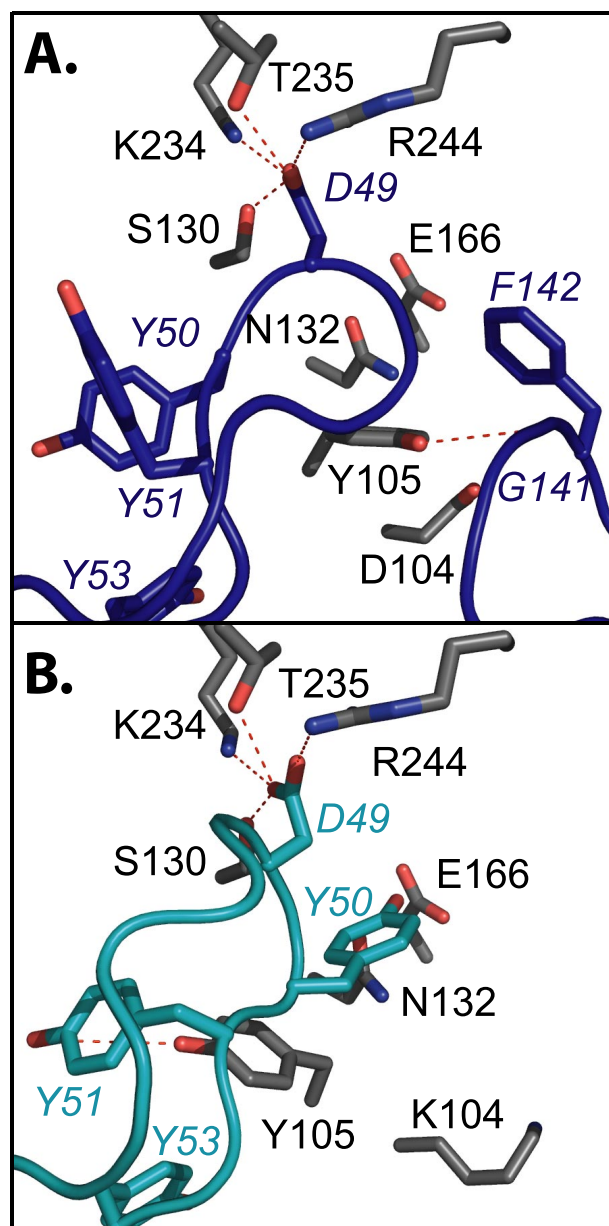


FIGURE 4. Structural changes at the  $\beta$ -lactamase-BLIP interface. A, interactions of the Asp-49 and Phe-142 loops of BLIP (dark blue) in complex with SHV-1 (gray). B, interactions of the Asp-49 and Phe-142 loops of BLIP (cyan) in complex with SHV-1 D104K (gray).

F142A·BLIP structure (13), in which the Asp-49 and Phe-142 loops maintain their positions in the active site, but the area around the Phe-142 loop is unstructured. Tyr-50<sub>BLIP</sub> also forms new interactions with Ser-130<sub>SHV</sub>, Asn-132<sub>SHV</sub>, and Glu-166<sub>SHV</sub>.

Examining the SHV·BLIP structures with PROCHECK reveals that Tyr-50<sub>BLIP</sub> is sterically strained in the wild type interface, and the altered conformation of the Asp-49 loop in the SHV D104K·BLIP structure relieves this strain (35). The Y50A mutation stabilizes both the TEM-1·BLIP and SHV-1·BLIP interfaces (2). This stabilizing effect may arise from relief of steric strain in the Asp-49 loop.

Summarizing, the Phe-142 loop swings out of the SHV active site cavity, whereas residues in the Asp-49 loop rotate in to

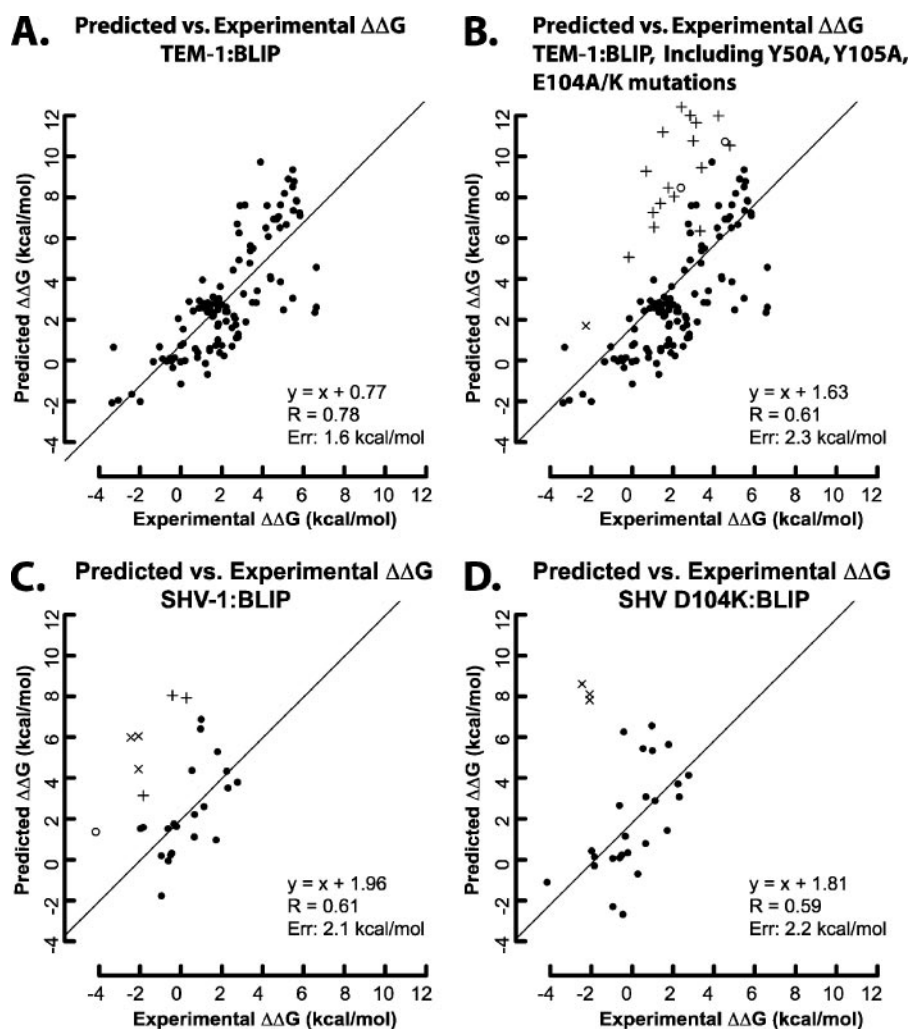


FIGURE 5. Correlation between predicted and experimental  $\Delta\Delta G_{d,mut}$  for TEM-1·BLIP and SHV-1·BLIP. *A*, correlation for TEM-1·BLIP interface mutations well described by the fixed backbone model. *B*, correlation for TEM-1·BLIP interface mutations, including those overpredicted by the fixed backbone model.  $\times$ , Y50A mutations;  $+$ , Y105A mutations;  $\circ$ , the E104K/F142A and E104A/F142A/K74A/Y143A mutations. *C*, correlation for SHV-1·BLIP mutations calculated with the SHV-1·BLIP structure.  $\times$ , Y50A mutations;  $+$ , Y143A/W112A, F142A, and E73A/Y143A mutations;  $\circ$ , the D104E mutation. *D*, correlation for SHV-1·BLIP mutations calculated with the SHV D104K·BLIP structure.  $\times$ , Y50A mutations.

occupy some of the missing positions. Newly created interactions from the Asp-49 loop and relief of steric strain may explain the slightly increased affinity of SHV D104K over SHV-1 for BLIP. These large concerted structural rearrangements also illustrate how prediction of the effects of mutations may sometimes be difficult. Nevertheless, since we are interested in using computational methods to guide future mutagenesis studies of the interface, we conducted an extensive examination of the ability of EGAD to predict stability changes arising from mutation.

**Calculation of  $\Delta\Delta G_{d,mut}$  Using EGAD**—Dissociation constants have been experimentally determined for an extensive set of both TEM-1·BLIP and SHV-1·BLIP mutant complexes, including nonalanine mutations and constructs with as many as six mutations (2, 7, 9, 11–14). These data provide an excellent opportunity for evaluating the ability of EGAD to calculate changes in the free energy of dissociation ( $\Delta\Delta G_{d,mut}$ ) and, where predictions fall short, a metric for improving the energy

function. Experimentally observed  $\Delta\Delta G_{d,mut}$  values were calculated within an error of 1.6 kcal/mol for a set of 112 TEM-1·BLIP mutants (Fig. 5A). By comparison, the experimental error for  $\Delta\Delta G_{d,mut}$  determined from independent experiments ranges from 0.1 to 1.3 kcal/mol (average 0.5 kcal/mol) for the TEM-1·BLIP interface. Whereas this demonstrates that the program performs reasonably well for the majority of characterized mutations, in several cases, we find the changes in energy to be largely overestimated.  $\Delta\Delta G_{d,mut}$  is consistently overpredicted for complexes that include BLIP Y50A or TEM Y105A. The calculated changes in affinity are also overpredicted for the double mutant TEM E104K·BLIP F142A and for the quadruple mutant TEM E104A·BLIP K74A/F142A/Y143A (Fig. 5B). For the SHV-1·BLIP interface, energies were calculated using the backbone conformations from both the SHV-1·BLIP and SHV D104K·BLIP complex structures. Using the SHV-1·BLIP structure, the effects of mutation on binding affinity are predicted within an error of 2.1 kcal/mol, and for the SHV D104K·BLIP structure, the error is 2.2 kcal/mol (Fig. 5, C and D). For both structures,  $\Delta\Delta G_{d,mut}$  is again overpredicted for complexes that include the mutation BLIP Y50A. Calculations using the SHV-1·BLIP structure also overpredicted the effects of mutants

BLIP F142A, BLIP Y143A/W112A, BLIP E73A/Y143A, and SHV D104E.

## DISCUSSION

Subtle structural differences between SHV-1 and TEM-1 result in a large change in BLIP binding affinity (Fig. 1, B–E). Four SHV-1 residues that differ in identity from TEM-1 result in decreased vdW and electrostatic interactions at the interface according to our calculations. These include Q100N, A114T, T167P, and D104E (SHV amino acid identity is listed first). Importantly, the loss of stabilizing interactions indicated by the structures and quantified with our program is in agreement with previous alanine scanning mutagenesis. For example, EGAD calculations find that the Q100N difference results in less extensive vdW contacts between Gln-100<sub>SHV</sub> and both Trp-150<sub>BLIP</sub> and Arg-160<sub>BLIP</sub> (supplemental Table 2). This provides a possible structural explanation for previous alanine scanning data, which found that the BLIP W150A and R160A

## Characterization of the SHV-1·BLIP Interface

mutations were far more destabilizing to the TEM-1·BLIP interface than the SHV-1·BLIP interface (2). At position Thr-167<sub>SHV</sub>, EGAD calculates a decrease in vdW interactions with Trp-162<sub>BLIP</sub> relative to Pro-167<sub>TEM</sub> (supplemental Table 2). Correspondingly, it was experimentally determined that the BLIP W162A mutation destabilizes the TEM-1·BLIP complex by 2.18 kcal/mol but destabilizes the SHV-1·BLIP complex by only 0.53 kcal/mol (2). Additionally, the SHV-1·BLIP structure confirms that Asp-104<sub>SHV</sub> is unable to participate in a salt bridge formed by Glu-104<sub>TEM</sub> and Lys-74<sub>BLIP</sub>; experimentally, it was found that the BLIP K74A mutation destabilizes the TEM-1·BLIP interface due to the loss of the salt bridge but not the SHV-1·BLIP interface, where the salt bridge is absent (2).

The decreased volume of Asp-104<sub>SHV</sub> not only removes a salt bridge but has potential implications for the stability of the Phe-142 binding loop. As described under “Results,” a number of contacts with the Phe-142 binding loop are removed; calculating the interfacial vdW interactions for the Phe-142 loop with EGAD reveals that the interactions eliminated between Asp-104<sub>SHV</sub>, Phe-142<sub>BLIP</sub>, and Tyr-143<sub>BLIP</sub> account for 41% of the overall vdW energy stabilizing the loop in the TEM-1·BLIP complex. The reduced role of Phe-142<sub>BLIP</sub> in the SHV-1·BLIP interface is consistent with the appearance of the alternate conformation observed in the SHV D104K·BLIP complex and the relative indifference in binding affinity to the removal of Phe-142<sub>BLIP</sub> from the active site cavity. The conformational flexibility observed in the Asp-49 and Phe-142 loops may contribute to the ability of BLIP to bind a range of  $\beta$ -lactamases. Structural plasticity in loop regions is a common motif in protein interfaces that bind multiple partners with high affinity (*e.g.* conformational flexibility in antibody loops results in specific recognition of diverse antigens) (36).

Overall, the change in both hydrogen bonding and vdW packing in the SHV D104K·BLIP interface reflects a shift toward increased stabilization around the Asp-49 loop and a reduced number of interactions with the Phe-142 loop. This reorganization suggests that SHV-1 may be inhibited by a reduced set of contacts with a single binding loop. This finding is promising for inhibitor development and reinforces the results of previous efforts to develop peptide inhibitors. Peptides corresponding to residues 46–51 of BLIP (the Asp-49 binding loop) were shown to bind TEM-1 and SHV-1 with affinities of 488 and 420  $\mu\text{M}$ , respectively (37). Random fragmentation and phage display of BLIP identified a peptide consisting of residues 30–49 of BLIP that inhibits TEM-1 with 446  $\mu\text{M}$  affinity, and a combination of phage display and peptide arrays identified a 136  $\mu\text{M}$  inhibitor that has 50% sequence identity to BLIP residues 46–51 (38, 39). All of these studies point to the central importance of the Asp-49 loop in inhibition.

The  $\beta$ -lactamase·BLIP complexes represent challenging computational analysis and design problems, since our structures indicate that the BLIP backbone assumes multiple conformations to accommodate mutations. With some notable exceptions (40–42), many computational design approaches use a fixed backbone approximation to simplify calculations. This approximation allows only side chain mobility, thus enormously reducing the degrees of conformational freedom required for the energy minimization. However, the fixed backbone approxima-

tion may introduce significant error into design calculations, since backbone adjustments upon mutation are neglected. Further, the possible coexistence of multiple conformations is ignored. Entropic effects, such as the penalty associated with burying a flexible loop in a protein-protein interface, are not accounted for. Despite the use of these approximations, the  $\Delta\Delta G_{d, \text{mut}}$  values of 85% of the TEM-1·BLIP complexes are predicted within 1.6 kcal/mol. For the SHV-1·BLIP complexes, the calculations are less successful. Using the SHV-1·BLIP structure as a backbone model,  $\Delta\Delta G_{d, \text{mut}}$  is overestimated for nearly 26% of the mutant complexes.

Mutations involving large changes in volume (*e.g.* tyrosine to alanine) at amino acid positions that undergo dramatic conformational changes between the SHV-1·BLIP and SHV-1 D104K·BLIP structures were frequently observed as outliers in both the TEM-1·BLIP and SHV-1·BLIP correlations. Neglecting backbone motion results in poor modeling of such mutations. Better treatment of loop conformational flexibility, possibly incorporating energy calculations over a backbone ensemble rather than use of a single fixed backbone, may be necessary for higher accuracy calculations (43, 44).

## CONCLUSION

A combination of structural, mutagenic, and computational analysis of the SHV-1·BLIP interface has highlighted several subtle yet important differences between this complex and that of TEM-1·BLIP. Notably, the region surrounding  $\beta$ -lactamase position 104 appears to be a key determinant of specificity. Creation of BLIP mutants that attempt to compensate for local interface differences near this and other positions may result in tighter binding variants. The reasonable success of EGAD in predicting the experimental mutational data suggests that it will be useful in guiding further mutagenesis efforts.

*Acknowledgments*—We thank Susan Jensen for the BLIP/pET26b construct. The TEM-1/pET24a(+) construct was a kind gift from Stéphane Gagné. We thank Marianne Carey for HPLC purification of the SHV D104K enzyme. We also thank Arnab Chowdry, Andrew Douglas, Melinda Hanes, Navin Pokala, and Mark Voorhies for useful discussions and advice.

## REFERENCES

1. Strynadka, N. C. J., Jensen, S. E., Johns, K., Blanchard, H., Page, M., Matagne, A., Frère, J.-M., and James, M. N. G. (1994) *Nature* **368**, 657–660
2. Zhang, Z., and Palzkill, T. (2004) *J. Biol. Chem.* **279**, 42860–42866
3. Kuzin, A. P., Nukaga, M., Nukaga, Y., Hujer, A. M., Bonomo, R. A., and Knox, J. R. (1999) *Biochemistry* **38**, 5720–5727
4. Zhang, Z., and Palzkill, T. (2003) *J. Biol. Chem.* **278**, 45706–45712
5. Strynadka, N. C. J., Jensen, S. E., Alzari, P. M., and James, M. N. G. (1996) *Nat. Struct. Biol.* **3**, 290–297
6. Ambler, R. P., Coulson, A. F., Frère, J. M., Ghuysen, J. M., Joris, B., Forshman, M., Levesque, R. C., Tiraby, G., and Waley, S. G. (1991) *Biochem. J.* **276**, 269–270
7. Petrosino, J., Rudgers, G., Gilbert, H., and Palzkill, T. (1999) *J. Biol. Chem.* **274**, 2394–2400
8. Joughin, B. A., Green, D. F., and Tidor, B. (2005) *Protein Sci.* **14**, 1363–1369
9. Selzer, T., Albeck, S., and Schreiber, G. (2000) *Nat. Struct. Biol.* **7**, 537–541
10. Selzer, T., and Schreiber, G. (2001) *Proteins Struct. Funct. Genet.* **45**,

- 190–198
11. Albeck, S., and Schreiber, G. (1999) *Biochemistry* **38**, 11–21
  12. Albeck, S., Unger, R., and Schreiber, G. (2000) *J. Mol. Biol.* **298**, 503–520
  13. Reichmann, D., Rahat, O., Albeck, S., Megeed, R., Dym, O., and Schreiber, G. (2005) *Proc. Natl. Acad. Sci. U. S. A.* **102**, 57–62
  14. Rudgers, G. W., and Palzkill, T. (1999) *J. Biol. Chem.* **274**, 6963–6971
  15. Pokala, N., and Handel, T. (2005) *J. Mol. Biol.* **347**, 203–227
  16. Hujer, A. M., Hujer, K. M., and Bonomo, R. A. (2001) *Biochim. Biophys. Acta* **1547**, 37–50
  17. Rice, L. B., Carias, L. L., Hujer, A. M., Bonafede, M., Hutton, R., Hoyen, C., and Bonomo, R. A. (2000) *Antimicrob. Agents Chemother.* **44**, 362–367
  18. Lin, S., Thomas, M., Shlaes, D. M., Rudin, S. D., Knox, J. R., V., A., and Bonomo, R. A. (1998) *Biochem. J.* **333**, 395–400
  19. Sosa-Peinado, A., Mustafi, D., and Makinen, M. W. (2000) *Protein Expression Purif.* **19**, 235–245
  20. MacDowell, A. A., Celestre, R. S., Howells, M., McKinney, W., Krupnick, J., Cambie, D., Domning, E. E., Duarte, R. M., Kelez, N., Plate, D. W., Cork, C. W., Earnest, T. N., Dickert, J., Meigs, G., Ralston, C., Holton, J. M., Alber, T., Berger, J. M., Agard, D. A., and Padmore, H. A. (2004) *J. Synchrotron Radiat.* **11**, 447–455
  21. Otwinowski, Z., and Minor, W. (1997) *Methods Enzymol.* **276**, 472–494
  22. Holton, J., and Alber, T. (2004) *Proc. Natl. Acad. Sci. U. S. A.* **101**, 1537–1542
  23. Leslie, A. G. W. (1992) *Joint CCP4 + ESF-EACBM Newsletter on Protein Crystallography* **26**
  24. Storoni, L. C., McCoy, A. J., and Read, R. J. (2004) *Acta Crystallogr. Sect. D Biol. Crystallogr.* **60**, 432–438
  25. Jones, T. A., and Kjeldgaard, M. (1997) *O: The Manual, Version 7.0*, Uppsala Software Factory, Uppsala, Sweden
  26. Lamzin, V. S., and Wilson, K. S. (1993) *Acta Crystallogr. Sect. D Biol. Crystallogr.* **49**, 129–147
  27. Winn, M. D., Isupov, M. N., and Murshudov, G. N. (2001) *Acta Crystallogr. Sect. D Biol. Crystallogr.* **57**, 122–133
  28. Kleywegt, G. J., and Jones, T. A. (1994) *Joint CCP4 + ESF-EACBM Newsletter Protein Crystallogr.* **31**, 9–14
  29. DeLano, W. L. (2002) *The PyMOL Molecular Graphics System*, DeLano Scientific, San Carlos, CA
  30. O'Callaghan, C., Morris, A., Kirby, S., and Shingler, A. (1972) *Antimicrob. Agents Chemother.* **1**, 283–288
  31. Pokala, N., and Handel, T. M. (2004) *Protein Sci.* **13**, 925–936
  32. Jorgensen, W. L., Maxwell, D. S., and Tirado-Rives, J. (1996) *J. Am. Chem. Soc.* **118**, 11225–11236
  33. Horn, J. R., and Shoichet, B. K. (2004) *J. Mol. Biol.* **336**, 1283–1291
  34. Word, J. M., Lovell, S. C., Richardson, J. S., and Richardson, D. C. (1999) *J. Mol. Biol.* **285**, 1735–1747
  35. Laskowski, R. A., MacArthur, M. W., Moss, D. S., and Thornton, J. M. (1993) *J. Appl. Crystallogr.* **26**, 283–291
  36. James, L. C., Roversi, P., and Tawfik, D. S. (2003) *Science* **299**, 1362–1367
  37. Rudgers, G. W., Huang, W., and Palzkill, T. (2001) *Antimicrob. Agents Chemother.* **45**, 3279–3286
  38. Huang, W., Beharry, Z., Zhang, Z., and Palzkill, T. (2003) *Protein Eng.* **16**, 853–860
  39. Rudgers, G. W., and Palzkill, T. (2001) *Protein Eng.* **14**, 487–492
  40. Harbury, P. B., Plecs, J. J., Tidor, B., Alber, T., and Kim, P. S. (1998) *Science* **282**, 1462–1467
  41. Kuhlman, B., Dantas, G., Ireton, G. C., Varani, G., Stoddard, B. L., and Baker, D. (2003) *Science* **302**, 1364–1368
  42. Offredi, F., Dubail, F., Kischel, P., Sarinski, K., Stern, A. S., Van de Weerd, C., Hoch, J. C., Proserpi, C., Francois, J. M., Mayo, S. L., and Martial, J. A. (2003) *J. Mol. Biol.* **325**, 163–174
  43. Kuhlman, B., O'Neill, J. W., Kim, D. E., Zhang, K. Y. J., and Baker, D. (2002) *J. Mol. Biol.* **315**, 471–477
  44. Larson, S. M., England, J. L., Desjarlais, J. R., and Pande, V. S. (2002) *Protein Sci.* **11**, 2804–2813
  45. Berman, H. M., Westbrook, J., Feng, Z., Gilliland, G., Bhat, T. N., Weissig, H., Shindyalov, I. N., and Bourne, P. E. (2000) *Nucleic Acids Res.* **28**, 235–242